ACS Partner Journal

CHEMICAL & BIOMEDICAL IMAGING

Open Access



pubs.acs.org/ChemBioImaging

Article

# Low-Frequency Coherent Raman Imaging Robust to Optical Scattering

*Published as part of Chemical & Biomedical Imaging virtual special issue "Sub-diffraction Chemical Imaging".*

David R. Smith, Jesse W. Wilson, Siddarth Shivkumar, Hervé Rigneault, and Randy A. Bartels*

Cite This: *Chem. Biomed. Imaging* 2024, 2, 584−591

Read Online

ACCESS | Metrics & More | Article Recommendations | Supporting Information

**ABSTRACT:** We demonstrate low-frequency interferometric impulsive stimulated Raman scattering (ISRS) imaging with high robustness to distortions by optical scattering. ISRS is a pump−probe coherent Raman spectroscopy that can capture Raman vibrational spectra. Recording of ISRS spectra requires isolation of a probe pulse from the pump pulse. While this separation is simple in nonscattering specimens, such as liquids, scattering leads to significant pump pulse contamination and prevents the extraction of a Raman spectrum. We introduce a robust method for ISRS microscopy that works in complex scattering samples. High signal-to-noise ISRS spectra are obtained even when the pump and probe pulses pass through many scattering layers.

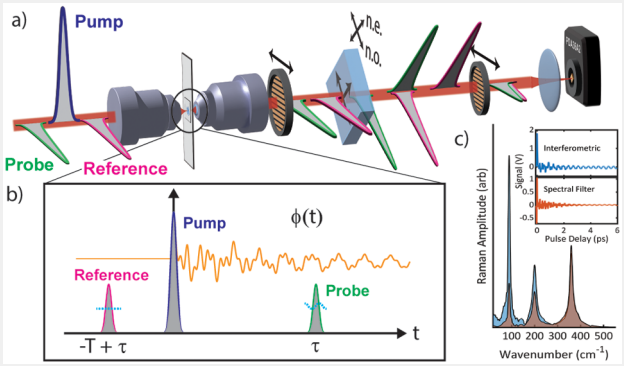


**KEYWORDS:** *coherent Raman, Raman microscopy, terahertz Raman, low frequency Raman, impulsive stimulated Raman scattering*

## INTRODUCTION

Chemical imaging is a powerful modality in the biological sciences. While fluorescent imaging with exogenous fluorescent probes or transgenically expressed fluorescent proteins forms the workhorse for targeted molecular imaging in biological specimens,[1] limitations of fluorescent imaging technologies have driven the development of label-free imaging modalities.[2−8] Of the many label-free imaging modalities, microscopy based on Raman scattering remains particularly appealing due to the narrow Raman vibrational spectroscopic lines that permit reliable identification of molecular species.

The vibrational frequency of materials and molecules offers a powerful means to both identify them and probe their dynamics and interactions.[5] Spectral features of the vibrational spectrum can be optically interrogated through either direct dipole-allowed transitions with infrared spectroscopy or inelastic Raman scattering. Raman scattering is often preferred because infrared spectroscopy suffers from interference from water absorption, broad spectral features, and low spatial resolution resulting from the use of long optical wavelengths.[8] That said, while Raman microscopy with spontaneous scattering is common for many applications, the weak Raman scattering cross-section and incoherent nature of spontaneous Raman scattering severely limit the rate of scattered signal detection—leading to long integration times and poor sensitivity to low concentrations of Raman-active molecules. Raman signals can be enhanced by stimulating the Raman transitions, either by introducing near-field enhancements or by directly stimulating the transitions with a Stokes laser field. Coherent Raman scattering (CRS)[2] overcomes the weak Raman signals by invoking stimulated Raman scattering to drive a much larger response, enabling video-rate CRS microscopy. Moreover, an improved detection sensitivity for low-concentration and weak Raman scattering modes is obtained with techniques that leverage homodyne interference, producing a linear dependence of the CRS signal on concentration.[2,9,10]

Raman vibrational frequencies carry extremely valuable information for the study of molecules and material systems. Vibrational frequencies, $\Omega_v$, scale as a harmonic oscillator, $\Omega_v^2 = k/m$. Thus, the strong binding, associated with a large value of the effective force constant $k$, and low (reduced) mass, $m$, of the vibrational mode correspond to high vibrational frequencies. The highest frequency modes are approximately localized and correspond to hydrogen bonds due to the low hydrogen mass and are used in investigations of water and lipids. The midband frequencies, $\Omega_v \approx 400-1200$ cm$^{-1}$, are extremely powerful for the identification of particular molecules[2] and even for bacterial classification.[11] Recent

**Received:** February 10, 2024
**Revised:** June 11, 2024
**Accepted:** June 14, 2024
**Published:** July 8, 2024

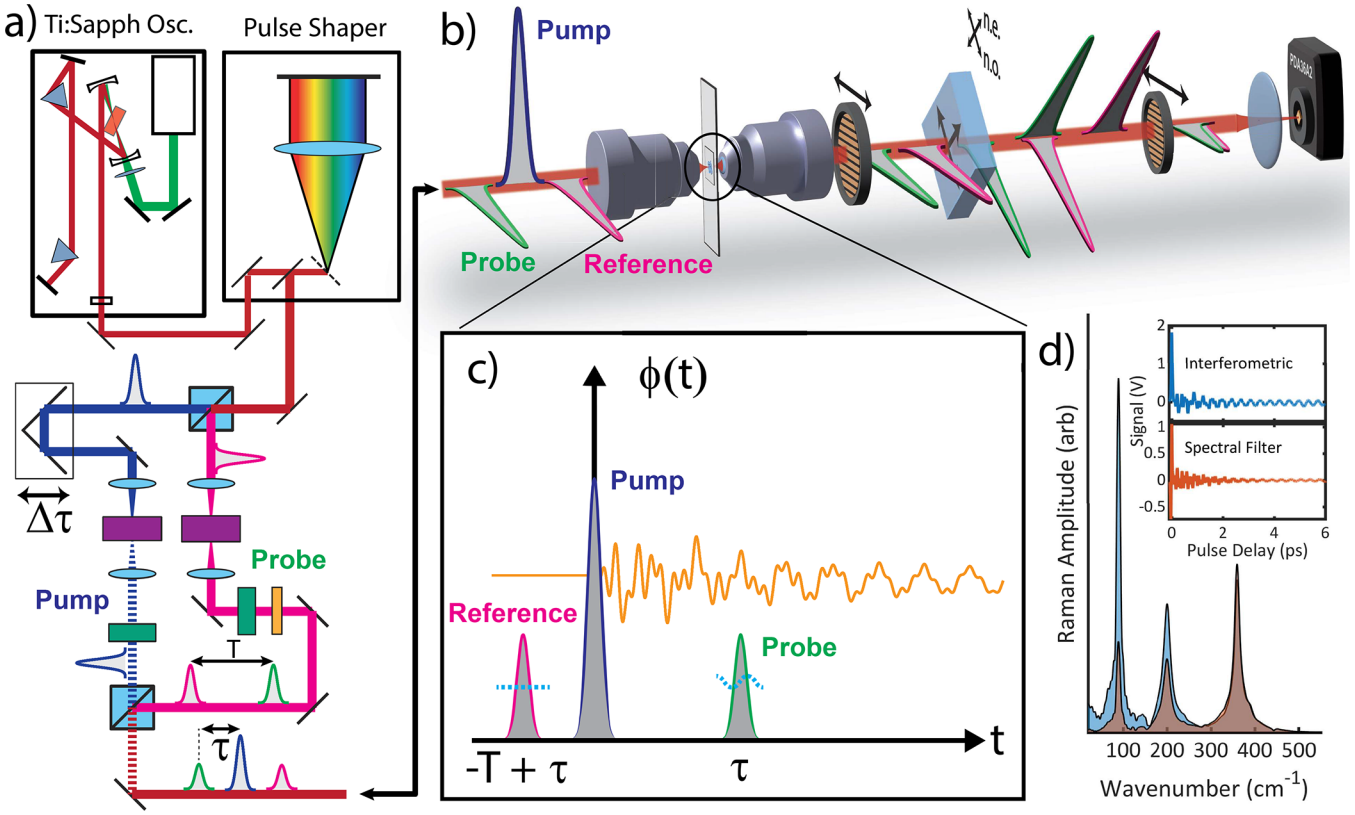


**Figure 1.** Common path interferometric $\phi$-ISRS concept figure. (a) Experimental setup for $\phi$-ISRS. The acousto-optic modulators, calcite crystals, and linear polarizer are represented by the purple, green, and orange elements, respectively. (b) Conceptual figure that shows the interaction of the pump, probe, and reference pulses with the sample as well as the isolation of the probe−reference pair and retiming to produce pulse interference. The interference produces signal current changes in a photodiode that are proportional to the Raman-induced transient phase, $\phi(\tau)$, at the arrival time, $\tau$, of the probe pulse. (c) The relative arrival time of the pump, probe, and reference pulses. (d) Example Raman spectra measured in BGO for $\phi$-ISRS and spectral shift detection.[32] The improved low-frequency Raman detection with $\phi$-ISRS is evident.

attention has focused on the largely neglected low-frequency vibrational modes.[9] These modes are generally associated with large reduced mass and correspond to vibrational motion that occurs over an extended region. Such relevant motions include virus capsid vibrations,[12] deformations of proteins,[13] and mechanical properties of solids, particularly for soft[14] and two-dimensional materials.[15,16]

However, implementation of Raman scattering at low vibrational frequencies remains a persistent challenge[9] because inelastic scattering at small offsets is difficult to measure, requiring low noise, narrow line width lasers, multiple stages of monochromators, and extremely steep spectral edge filters. The result is that imaging is extremely challenging. In this article, we introduce a simple and robust technique that is suitable for imaging in complex specimens. Our approach makes use of impulsive stimulated Raman scattering (ISRS) to probe low-frequency vibrational modes with time-domain spectroscopy.[9] In ISRS, a short pump pulse is used to drive the excitation of vibrational coherences for vibrational frequencies lower than $\sim 1/\tau_p$, where $\tau_p$ is the pump pulse duration.[17] Because the Raman interaction involves a change in molecular polarizability with vibrational displacement, excitation of vibrational coherences produces an effective time-varying perturbation to the linear optical susceptibility denoted by $\delta\chi_{eff}(t)$.[9] The Raman spectrum is obtained by recording signals with a probe pulse that follows behind the pump pulse by a delay of $\tau$. The recorded signals are derived from the temporal phase, $\phi_v(t)$, accumulated by the probe pulse as it propagates through the excited vibrational coherence. This recovered spectrum is continuous and spans a range with a maximum frequency on the order of $1/\tau_p$ down to a minimum frequency $1/\Delta\tau$ bounded by the range of pump−probe delay $\Delta\tau$.

The readout method of the Raman spectrum in ISRS impacts the sensitivity of spectral detection.[9] The most common technique is to make use of a spectral shift for detection, where spectral scattering from the time-dependent phase modulation applied to the probe pulse by the transient effective linear optical susceptibility leads to changes in power transmitted through a spectral filter.[18−21] Improved detection sensitivity can be achieved by turning the probe pulse spectral shift into a change in arrival time at a detector by applying additional spectral dispersion.[22] Methods that detect the signal based on a spectral shift reduce the amplitude of the low-frequency vibrational modes and impart an effective spectral filter on the relative amplitudes of the Raman spectrum. To emphasize the low-frequency vibrational modes and eliminate the spectral distortions imparted by frequency shift detection, $\delta\chi_{eff}(\tau)$ should be probed directly.[9]

Low-frequency vibrations can be readily detected with ISRS methods where the signal detection is directly proportional to the time-varying change in the optical susceptibility induced by the forced Raman response. Several methods have been explored for the direct measurement of $\delta\chi_{eff}(t)$ to obtain an undistorted Raman spectrum, which we call phase-sensitive ISRS ($\phi$-ISRS). $\phi$-ISRS spectroscopy was originally implemented in a transient grating geometry,[17] which allows for


https://doi.org/10.1021/cbmi.4c00020
Chem. Biomed. Imaging 2024, 2, 584−591

background-free measurements but relies on direct measurement of the diffracted beam power, leading to limited detection sensitivity. In the transient grating experiment, the amplitude of the diffracted probe field is proportional to $\delta\chi_{\text{eff}}(\tau)$, i.e., the susceptibility perturbation at the pump−probe delay $\tau$. However, because the total scattered power is recorded, the Raman spectrum is distorted. The direct amplitude of $\delta\chi_{\text{eff}}(\tau)$ can be obtained with Kerr lensing[23] and interferometric measurements.[24−28] A comparison of the Raman spectral amplitudes has been demonstrated in a Sagnac interferometer configuration and verified the access to low-frequency vibrational spectral information when $\delta\chi_{\text{eff}}(t)$ is directly obtained with an enhancement in the signal strength for low-frequency measurements compared to a frequency shift;[24] this result has recently been validated in further experiments.[28] The Sagnac interferometer configuration is intrinsically stable but has limited application for spectroscopic or imaging measurements. A stable common path interferometer configuration is possible with a collinear time-delayed probe and reference pulse configuration,[29,30] which has been demonstrated with spectral interferometry[25−27] and Fourier transform interferometry.[31]

## CONCEPT

Unfortunately, the existing $\phi$-ISRS methods are restricted to nondepolarizing and nonscattering samples such as liquid-phase spectroscopy or transparent crystals. In this article, we introduce a simple collinear interferometric approach to $\phi$-ISRS that is extremely stable and thus performs robustly in the presence of strong scattering and depolarization effects, such as in cell culture and tissues.

A conceptual schematic of the experimental system is shown in Figure 1. A mode-locked ultrafast laser produces pulses that are passed through a spatial light modulator pulse shaper for second- and third-order dispersion control. The laser beam power is split into pump and probe pulses in an orthogonally polarized Mach−Zenhder interferometer. The pump pulse intensity is modulated by an acousto-optic modulator to allow for lock-in amplifier detection of the Raman signal. A computer-controlled resonant delay scanner in the pump arm enables rapid scanning of the relative pump−probe delay $\tau$. The probe pulse arm is modified from a standard pump−probe experimental arrangement[19,21,33] in order to generate a probe−reference pulse pair with a birefringent optical crystal.[30]

Birefringent crystals are used both as a pulse pair generator[19,30,34] and a pulse retimer to create a common path collinearly propagating probe−reference pulse pair with an extremely stable relative phase and a temporal separation of $T$, as shown in Figure 1b. The probe−reference pair is generated by sending a linearly polarized probe pulse through a birefringent crystal plate rotated so that the eigenpolarization axes are at 45° with respect to the input linear polarization of the probe pulse. Depending on the cut of the crystal and the orientation of the optic axis, the relative delay time, $T$, can be adjusted by rotating the birefringent crystal or by adjusting the crystal thickness. The pulses are separated by a few picoseconds and share a common propagation path.

To combine the probe−reference pulse pair with the pump pulse, the probe−reference pair is projected onto the same linear polarization axis in the polarizing beam splitter where the pulse pair is combined with the orthogonally polarized pump pulse. The pulses are focused into the sample with a high numerical aperture aspheric lens and recollimated with an identical aspheric lens after passing through the specimen. The pump pulse is removed from the collimated beams with a polarizer to isolate the probe−reference pulse pair.

The coherent ISRS signal is contained in a phase perturbation, $\phi_v(t)$, induced by the pump pulse. The reference pulse precedes the pump pulse, accumulating a phase as it propagates through the optical system. This phase accumulated by the reference pulse comes from the sample at equilibrium because the vibrational coherences decay to equilibrium (over several picoseconds), long before the next pulse in the oscillator pulse train arrives (∼10 ns). By contrast, the probe pulse arrives at a delay, $\tau$, after the pump pulse and accumulates a phase identical with the reference pulse in addition to a phase perturbation induced by Raman excitation by the pump pulse. By placing the pump pulse in between the reference and the probe pulses, the relative phase between the probe and the reference pulses is the accumulated vibrational phase perturbation acquired by the probe pulse. After interacting with the sample, the probe−reference pair is isolated from the pump pulse, for example, with a polarizer; then, the probe−reference pulse pair is retimed. In this way, the relative phase is converted to an amplitude modulation through interference between the probe and the reference pulse so that the Raman signal is detected with a simple photodiode.

This pulse pair is retimed using a second birefringent crystal that is oriented at −45° to undo the probe−reference delay so that the probe and reference pulses overlap in time, i.e., setting $T = 0$. Because the probe−reference pulse pair propagates along the same direction and are only separated by a few picoseconds, $T \approx 6$ ps, the relative phase between these two pulses is exceptionally stable, allowing very stable phase measurements of the transient phase introduced by the pump pulse. The probe and reference pulses are in the same spatial mode and polarization state; however, only one-half of the power of the probe and reference pulses is overlapped in time and will interfere (see Figure 1b)). Because, the two pulses travel through exactly the same optical path and thus share the same spatial mode, making interference between the beams robust to perturbations acquired with propagation through optical scattering environments. To demonstrate the robustness of our approach, we introduce controlled scattering to a sample by adding layers of parafilm on the sample between the objective and the sample of interest. For a more detailed description of the experimental setup, please refer to the Supporting Information

The interferometric signal for ISRS spectroscopy emerges from the fact that the pump pulse excites a nonequilibrium time-varying change in effective linear optical susceptibility, $\delta\chi_{\text{eff}}(t)$, imparting a transient phase modulation on a time-delayed probe pulse. The reference pulse can be arranged to arrive before the pump pulse so that the only phase that it accumulates is from the optical system and the specimen at thermal equilibrium. The pump pulse-induced phase perturbation, $\phi_v(t) = k_{\text{pr}} l \delta\chi_{\text{eff}}(t)/2n_0$, is then the only phase shift acquired between the probe and the reference pulses. Here, $l$ is the focal interaction length, $n_0$ is the sample refractive index at thermal equilibrium, and $k_{\text{pr}} = 2\pi/\lambda$ is the free-space wavenumber for a pulse with center wavelength $\lambda$. The fact that the probe and reference pulses are common path means that all accumulated scattering, aberrations, and depolariza-


https://doi.org/10.1021/cbmi.4c00020
Chem. Biomed. Imaging 2024, 2, 584−591

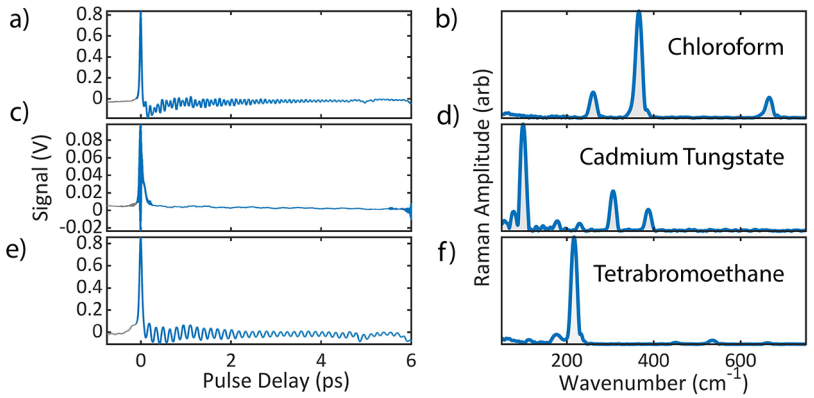


**Figure 2.** $\phi$-ISRS data from multiple samples with low-frequency Raman vibrations. (a) The time-resolved $\phi$-ISRS signal for chloroform. (b) The recovered Raman spectrum of chloroform. (c and d) Time-resolved signal and Raman spectrum for cadmium tungstate. (e and f) Time-resolved signal and Raman spectrum for tetrabromoethane. Liquid and depolarizing crystal samples illustrate the effectiveness of $\phi$-ISRS for robust low-frequency Raman spectroscopy.

tions are identical for both beams. This produces an extremely stable signal that prevents many forms of technical noise.

The phase modulation due to the excited vibrational coherence can be expressed as a linear superposition of the phase modulation from each excited vibrational mode as $\delta\phi^{v}(\tau)=\sum_{v}\delta\phi_0^{v}h_v(\tau)$ and depends on the arrival time $\tau$ of the probe pulse after the excitation induced by the pump and is summed over the contribution of each vibrational mode, denoted with a superscript v. Each vibrational mode is excited through an impulsive forced Raman response that is driven by the pump pulse, leading to a damped causal oscillation,[9,10] $h_v(t) = \Theta(t)\exp(-\Gamma_v t/2)\sin(\Omega_v t)$. Here, $\Theta(t)$ is the Heaviside step function that ensures causality and $\Gamma_v$ is the damping rate of the mode at the vibrational frequency $\Omega_v$. The induced vibrational phase perturbation $\delta\phi_0^{v} = g_f \mathrm{Im}[\chi_{VR}^{(3)}(\Omega_v)]\Gamma_v\tilde{D}(\Omega_v)\overline{p}_{pu}$ scales linearly with the average power of the pump pulse, $\overline{p}_{pu}$, and the molecular concentration, $N$, which becomes clear when we note that $\mathrm{Im}[\chi_{VR}^{(3)}(\Omega_v)]=N(\partial\alpha/\partial Q)_0^2/6\epsilon_0\Gamma_v\Omega_v$. The amplitude of the Raman-induced phase modulation is also proportional to the power spectral density (PSD) of the pulse intensity profile at the vibrational frequency $\Omega_v$,[32,35] $\tilde{D}(\Omega) = \mathcal{F}\{I(t)\}/I_0\tau_0$. Here, $I_0$ is the peak pulse intensity and $\tau_0 = \int I(t)/I_0\,dt$ is a measure of the pulse duration. In the limit of an impulsive pump pulse, $I(t) = I_0\delta(t)$; then, the excitation PSD, $\tilde{D}(\Omega) \to 1$, so that the forced Raman response is the impulse for vibrational excitation. Here, we assume that the temporal duration, $\tau_p$, and the temporal intensity, $I(t)$, of the pump, probe, and reference pulses are all identical. The coherent Raman excitation that drives the vibrational phase perturbation also depends on the focusing conditions, which are encapsulated in the focusing parameter $g_f = 12\pi l/(n^2\epsilon_0 c\nu_R\mathcal{A}_f\lambda)$, where $\mathcal{A}_f$ is the focal beam cross sectional area, $\nu_R$ is the laser repetition rate frequency, and $\lambda$ is probe pulse center wavelength.

## RESULTS

In our experiment, the probe−reference pulse pair, with a total average power of $\overline{p}_{pr}$, is isolated from the pump pulse using a polarizer to block the pump pulse. Then, one-half of the probe and reference pulse average power is adjusted to interfere in a compact, collinear interferometer using an angle-tuned birefringent crystal. The relative phases of the probe and reference pulses are adjusted to be in quadrature so that the total power of the interfering pulses is $\overline{p}_{int} = \overline{p}_{pr}\{1 + \sin[\delta\phi^{v}(\tau)]\}/2$, leading to a signal power incident on the detector of $\overline{p}_{sig}(\tau) = \delta\phi^{v}(\tau)\overline{p}_{pr}/2$, with a background power equal to the total average probe pulse train power $\overline{p}_{bkg} = \overline{p}_{pr}$. In the shot noise limit, the signal-to-noise ratio (SNR) for a detection integration time of $\Delta t$ reads $\mathrm{SNR} = (\delta\phi^{v}/2)\Upsilon\sqrt{\Delta t}$, where $\Upsilon = \sqrt{\mathcal{R}\overline{p}_{pr}/e}$, $\mathcal{R}$ is the detector responsivity and $e$ is the elementary charge. Provided that the total probe power exceeds approximately 2 mW, the shot noise limit is valid for lock-in detection that is able to largely avoid the laser intensity fluctuation noise. Because both the signal power and the SNR depend linearly on $\delta\phi^{v}$, this collinear interferometric method is sensitive to low Raman vibrational frequencies and is limited where the impulsive Raman excitation strength, $\tilde{D}(\Omega_v)$, becomes too low, which occurs when the vibrational period is on the order of or larger than the pump pulse duration.

The $\phi$-ISRS spectrum of the low-frequency optical phonon Raman spectrum in BGO is shown in Figure 3d in comparison to a spectral shift measurement. The increased amplitude at low vibrational frequencies is apparent in the interferometric measurement. Because the pump−probe delay $\tau$ can be controlled independently of the separation between the probe and the reference pulses, which is a fixed delay $T$, there are three zones for the $\phi$-ISRS experimental system, each of which is illustrated in Figure S2. We define the time frame so that $t = 0$ occurs at the center of the pump pulse The first pulse to arrive is denoted the reference pulse that is incident at a time $t = \tau - T$, and the probe pulse arrives at a time $\tau$. Zone I occurs when $\tau < 0$, so that both the probe and the reference pulses arrive before the pump pulse. In this region, there is no pump-induced transient phase acquired between the probe and the reference pulses, so we have a null signal. Zone II is where we pull the Raman spectra; this temporal signal provides a pure Raman spectrum because only the probe pulse accumulated the Raman-induced phase shift. In Zone III, the spectrum is distorted because the interference signal is determined by the phase shift acquired by the probe and reference pulses, i.e., $\phi(\tau) - \phi(T - \tau)$.

Interferometric $\phi$-ISRS spectra from several samples displaying low-frequency Raman modes are shown in Figure


https://doi.org/10.1021/cbmi.4c00020
Chem. Biomed. Imaging 2024, 2, 584−591

2. While the chloroform and tetrabromoethane are liquid samples and do not suffer depolarization, the cadmium tungstate is a birefringent crystal and induces a depolarization between the pump pulse and the probe−reference pulse pair. The time-domain traces are shown on the left column, whereas the Raman spectra shown in the right column are computed from the power spectral density of the time-domain trace after isolation of the signal that contains only the Raman transients away from the cross phase modulation feature near time zero.[27] The observed Raman spectral modes match known Raman spectral lines of these three samples.

Hyperspectral Raman images of anthracene crystals for three low-frequency Raman-active optical phonon modes are shown in Figure 3. The Raman spectrum of the optical phonon modes

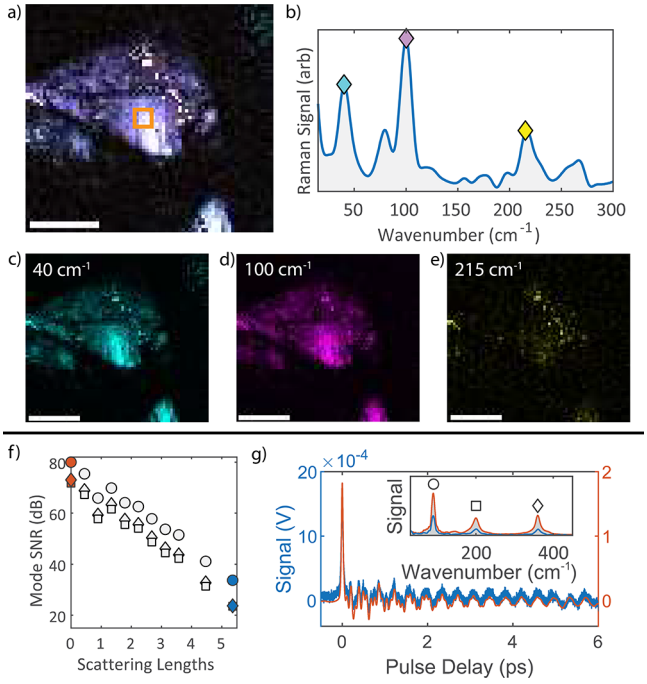


**Figure 3.** (a) Composite image of the three low-frequency Raman-active optical phonon modes in an anthracene crystal. (b) Raman spectrum of the crystal at a single pixel centered in the orange square shown in a. (c−e) Individual images of the three Raman modes indicated in b. (f) Signal-to-noise ratio (SNR) of the three Raman vibrational modes of a BGO crystal with scattering layers added between the sample and the excitation objective. A high SNR is indicated for >7 scattering lengths. (g) Comparison of the Raman spectrum of BGO for 0 and 12 scattering layers shows high-quality spectra extracted even under conditions of strong optical scattering. Image acquisition parameters and SNR calculation details can be found in the Supporting Information. Scale bar is 50 $\mu$m.

is shown in Figure 3b. Images for the three phonon modes marked in the spectrum are shown in Figure 3c−e, whereas a composite image is displayed in Figure 3a. The complex morphology of the crystals produces scattering that distorts the beams and degrades the Raman signal. However, we see that high-quality images are obtained with the common-path interferometric readout because the probe and reference pulses maintain identical spatial and polarization modes.

To quantitatively evaluate the effect of optical scattering on $\phi$-ISRS with common-path interferometric detection, we captured Raman spectra as we added layers of optical scattering material. For each measurement, the Raman signal and the noise were estimated using the power spectral density (PSD) of the time-resolved signal. The "signal" (S) for a known Raman mode is calculated from the root-mean-square (RMS) of the spectral mode whose width is determined by where the value drops to 95% of the mode peak. The "noise" (N) is calculated from the RMS of the PSD of a frequency region well removed from the Raman spectrum at wavenumbers above those excited by the pump pulse. From these values, we compute SNR = $10\log_{10}(S/N)$. To introduce optical scattering, layers of parafilm were added on the front of the BGO sample, thus introducing scattering before Raman excitation by the pump pulse and spectral scattering of the probe pulse. Results are shown in Figure 3f, displaying the SNR as a function of the number of scattering layers added between the sample and the excitation objective. The data show exponential decay of the SNR as a function of the number of scattering lengths. The Raman spectra for the highest and lowest SNR data are shown in Figure 3g.

## DISCUSSION

Imaging of low-frequency vibrational modes with coherent Raman remains a challenging prospect. Here, we introduce a new imaging strategy for a wide bandwidth of Raman vibrational frequencies, spanning from very low frequencies (<300 cm$^{-1}$) to frequencies well within the fingerprint region > 1000 cm$^{-1}$. Our new strategy relies on a pump−probe geometry using $\phi$-ISRS excitation of a vibrational coherence by a short pump pulse that is electronically nonresonant with the specimen. Such short pulse excitation is capable of exciting vibrational frequencies with periods that are longer than the pump pulse duration.[32] As a result, short laser pulses with carefully maintained dispersion compensation are critical for ISRS excitation. After excitation of the vibrational coherence, the readout of the signal with a probe pulse plays a crucial role in the vibrational frequencies that are observed. The conventional strategy is to use a spectral edge filter to convert the spectral scattering driven by the transient phase modulation acquired by the probe pulse when propagating through the vibrational coherence into a change in probe pulse power transmitted through the spectral filter.[19,36] Unfortunately, this simple strategy renders ISRS largely insensitive to low-frequency vibrations.[9] By reading out the phase directly through interferometry, we directly detect the time-domain-forced Raman response, providing sensitive detection of the low-frequency Raman vibrational modes.

Aside from the high sensitivity to low-frequency vibrational modes (e.g., terahertz Raman), we have demonstrated that our common-mode strategy for the detection of the transient Raman phase modulation produces high SNR data even in the face of optical scattering. This resilience of our signal detection to optical scattering follows from two properties that we acquire by generating the probe−reference pair in a suitably oriented birefringent crystal. The first property is that the probe and reference pulses share a common path. Because of this common path propagation, any scattering that is encountered is common to both the probe and the reference pulse beams. As a result, the beams are guaranteed to still interfere. Indeed, even depolarization is not a problem, as the spatial modes of the probe and reference beams are identical, ensuring stable interference even after becoming severely distorted, as they are distorted identically.

Of course, common path perturbations are only relevant if the relative phase, scattering, and depolarization are stable for


https://doi.org/10.1021/cbmi.4c00020
Chem. Biomed. Imaging 2024, 2, 584−591

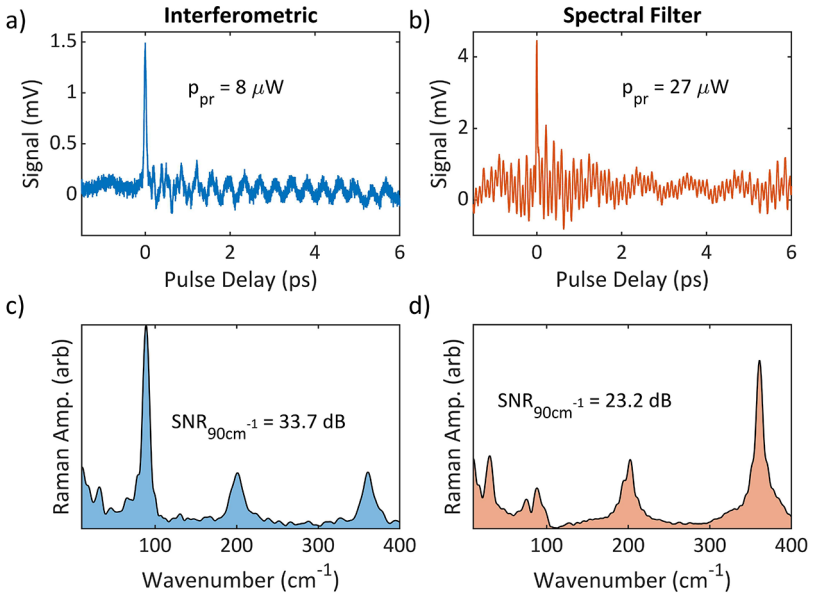


**Figure 4.** Comparison between $\phi$-ISRS and spectral filter detection ISRS through 12 scattering layers. (a) Time-resolved signal for $\phi$-ISRS with the probe power incident on the photodiode indicated. (b) Time-resolved signal for spectral filter detection ISRS with the probe power incident on the photodiode indicated. The time-resolved signal shows evidence of scattering and depolarization of the pump beam causing signal contamination around $\tau = 0$. (c and d) Raman spectra with the SNR of the 90 $cm^{-1}$ mode. Details of the SNR calculation can be found in the Supporting Information. $\phi$-ISRS shows a significantly higher SNR with a lower incident probe power. The pump contamination present in b and d contributes to distortion in the low-frequency spectrum in addition to the lower SNR.

the duration of the integration time over which the interference is acquired. The relative stability of the probe and reference pulses is guaranteed by the fact that there is very little perturbation of the refractive index of the specimen that can occur on the time scale of a few picoseconds other than the nonequilibrium vibrational coherence dynamics that are excited with the pump pulse.

The combination of the temporal and common-mode interferometric stability ensures extremely stable and high-sensitivity detection of the vibration-induced phase shift. The robustness of our approach is demonstrated by introducing controlled scattering to a sample by adding layers of parafilm on the sample between the objective and the sample of interest. The scattering introduced by the parafilm layers was characterized by measuring power transmission through a blank sample as more layers of parafilm were added. The power transmitted through the scattering layers decreases exponentially with the number of scattering layers. The scattering length, defined as when the optical power decreases by $1/e$, was found to be $l_s = 1.68$ parafilm layers. The scattering length was determined in a separate experiment where parafilm layers were sequentially added to a glass slide, and the transmitted power through the collection objective was directly measured with a power meter. Figure 3f shows the SNR for the three main vibrational modes of BGO as a function of scattering length of parafilm added to the sample. Figure 3g shows the time-resolved signal and the Raman spectrum (inset) of BGO with no scattering layers (orange) and the signal with the maximum number of scattering layers used (blue), which is 12 layers of parafilm, or 7.14 scattering lengths. This result shows the robustness of the interferometric Raman technique with the SNR of the BGO modes remaining high after over 7 scattering lengths. The incident optical powers incident on the sample were $p_{pu}$ = 37.8 mW and $p_{pr}$ = 38.95 mW for the pump and probe, respectively. After passing through the sample, objectives, retiming crystal, and analyzing polarizer, the probe power incident on the detection photodiode was $p_{pr}$ = 8.6 mW with no scattering present. The probe power incident on the detection photodiode was measured to be $p_{pr}$ = 8 $\mu$W with 12 parafilm layers (7.14 scattering lengths).

The pump−probe pulses are orthogonally polarized and we observe that the interferometric approach demonstrated here allows for more robust elimination of the pump pulse compared to the spectral filter method. This capability is evident in Figure 4, where the temporal signal for the interferometric approach in this present work generates a clean data trace, whereas the spectral filter version in Figure 4b exhibits pump contamination. The resulting spectrum of the Raman signal is much higher for the interferometric case (Figure 4c) than the spectral filter case (Figure 4d). Because we have constructed this system based on orthogonally polarized pump and probe−reference pulses, we are limited to vibrational modes with a more symmetric character and we may have reduced sensitivity to asymmetric modes. The spectral resolution of this strategy is limited to $\sim 1/T$ for methods that rely on power spectral estimation, e.g., the FFT or multitaper computation. However, the use of model-based estimation, e.g., LP-SVD, can circumvent this spectral resolution limitation. The lower bound of the vibrational frequency is limited by the scan range of the probe−reference pair. For Zone II, the lower bound is $\tilde{\nu} = (cT)^{-1} \approx 7$ $cm^{-1}$, but this can be extended arbitrarily with synthetic aperture scanning,[25] where the probe and reference pulse pair both follow the pump pulse, at the cost of the loss of frequencies with vibrational periods that are an integer multiple of $T$. Application of LD-SVD methods are expected to further improve this lower bound.


https://doi.org/10.1021/cbmi.4c00020
Chem. Biomed. Imaging 2024, 2, 584−591

## CONCLUSIONS

We have developed a new and versatile method for low-frequency coherent Raman imaging. Balanced detection could eliminate the need for the acousto-optic modulator for beam intensity modulation, which will drastically reduce the spectral dispersion burden of the system. Such an approach would allow for easier use of high numerical aperture objective lenses that also carry a high dispersion. Right now, the relatively low numerical aperture and off-axis aberrations of the aspheres have limited our ability to image in complex samples, and the long working distance makes thin samples such as two-dimensional materials challenging to image. Future advances will explore additional strategies to simplify the imaging approach.

## ASSOCIATED CONTENT

### Supporting Information

The Supporting Information is available free of charge at https://pubs.acs.org/doi/10.1021/cbmi.4c00020.

LaTex files and figure for the Supporting information (ZIP)

Render LaTex in the ZIP (PDF)

## AUTHOR INFORMATION


### Corresponding Author

**Randy A. Bartels** − *Biomedical Imaging, Morgridge Institute for Research, Madison, Wisconsin 53715, United States; Department of Biomedical Engineering, University of Wisconsin, Madison, Wisconsin 53715, United States;* orcid.org/0000-0003-0530-0435; Phone: 608-316-4100; Email: rbartels@morgride.org

### Authors

**David R. Smith** − *Biomedical Imaging, Morgridge Institute for Research, Madison, Wisconsin 53715, United States*

**Jesse W. Wilson** − *Department of Electrical Engineering and School of Biomedical Engineering, Colorado State University, Fort Collins, Colorado 80523, United States;* orcid.org/0000-0002-2237-9408

**Siddarth Shivkumar** − *Aix Marseille University, CNRS, Centrale Med, Institut Fresnel, Marseille 13397, France; Department of Physics, University of Ottawa, Ottawa, Ontario K1N6N5, Canada*

**Hervé Rigneault** − *Aix Marseille University, CNRS, Centrale Med, Institut Fresnel, Marseille 13397, France;* orcid.org/0000-0001-6007-0631

Complete contact information is available at: https://pubs.acs.org/10.1021/cbmi.4c00020


### Notes

The authors declare no competing financial interest.

## ACKNOWLEDGMENTS

We are grateful for the help of Dekel Raanan and Maor Asher for crystal synthesis as well as Dan Oron for helpful discussions and assistance with the sample. We are grateful for funding from DE-FOA-0002603 (R.A.B.). Alicia Williams from the Morgridge Institute provided scientific editing support. We acknowledge support from ANR-21-ESRS-0002 IDEC, EU ICT 101016923 CRIMSON, EU EIC 101099058 VIRUSONG, and EU ERC 101052911 (H.R.) and NIH 5 R21GM135772-02 (J.W.W. and R.A.B.).

## REFERENCES


(1) Thorn, K.; Kellogg, D. A quick guide to light microscopy in cell biology. *Mol. Biol. Cell* **2016**, *27*, 219−222.

(2) Tong, L.; Cheng, J.-X. Label-free imaging through nonlinear optical signals. *Mater. Today* **2011**, *14*, 264−273.

(3) Kasprowicz, R.; Suman, R.; O'Toole, P. Characterising live cell behaviour: Traditional label-free and quantitative phase imaging approaches. *International Journal of Biochemistry & Cell Biology* **2017**, *84*, 89−95.

(4) Cicchi, R.; Pavone, F. S. Multimodal nonlinear microscopy: A powerful label-free method for supporting standard diagnostics on biological tissues. *Journal of Innovative Optical Health Sciences* **2014**, *07*, 1330008.

(5) Schie, I. W.; Huser, T. Label-Free Analysis of Cellular Biochemistry by Raman Spectroscopy and Microscopy. *Comprehensive Physiology* **2013**, *3*, 941−956.

(6) Borile, G.; Sandrin, D.; Filippi, A.; Anderson, K. I.; Romanato, F. Label-Free Multiphoton Microscopy: Much More Than Fancy Images. *Int. J. Mol. Sci.* **2021**, *22*, 2657.

(7) Mazumder, N.; Balla, N. K.; Zhuo, G.-Y.; Kistenev, Y. V.; Kumar, R.; Kao, F.-J.; Brasselet, S.; Nikolaev, V. V.; Krivova, N. A. Label-Free Non-linear Multimodal Optical Microscopy—Basics, Development, and Applications. *Front. Phys.* **2019**, *7*, 170.

(8) Schnell, M.; Mittal, S.; Falahkheirkhah, K.; Mittal, A.; Yeh, K.; Kenkel, S.; Kajdacsy-Balla, A.; Carney, P. S.; Bhargava, R. All-digital histopathology by infrared-optical hybrid microscopy. *Proc. Natl. Acad. Sci. U. S. A.* **2020**, *117*, 3388−3396.

(9) Bartels, R. A.; Oron, D.; Rigneault, H. Low frequency coherent Raman spectroscopy. *Journal of Physics: Photonics* **2021**, *3*, 042004.

(10) Rigneault, H.; Berto, P. Tutorial: Coherent Raman light matter interaction processes. *APL Photonics* **2018**, *3*, 091101.

(11) Strola, S. A.; Baritaux, J.-C.; Schultz, E.; Simon, A. C.; Allier, C.; Espagnon, I.; Jary, D.; Dinten, J.-M. Single bacteria identification by Raman spectroscopy. *Journal of Biomedical Optics* **2014**, *19*, 111610.

(12) Tsen, K.-T.; Dykeman, E. C.; Sankey, O. F.; Tsen, S.-W. D.; Lin, N.-T.; Kiang, J. G. Probing the low-frequency vibrational modes of viruses with Raman scattering—bacteriophage M13 in water. *Journal of biomedical optics* **2007**, *12*, 024009.

(13) Rischel, C.; Spiedel, D.; Ridge, J. P.; Jones, M. R.; Breton, J.; Lambry, J.-C.; Martin, J.-L.; Vos, M. H. Low frequency vibrational modes in proteins: Changes induced by point-mutations in the protein-cofactor matrix of bacterial reaction centers. *Proc. Natl. Acad. Sci. U. S. A.* **1998**, *95*, 12306−12311.

(14) Amin, S.; Blake, S.; Kenyon, S. M.; Kennel, R. C.; Lewis, E. N. A novel combination of DLS-optical microrheology and low frequency Raman spectroscopy to reveal underlying biopolymer self-assembly and gelation mechanisms. *J. Chem. Phys.* **2014**, *141*, 234201.

(15) Sriv, T.; Kim, K.; Cheong, H. Low-Frequency Raman Spectroscopy of Few-Layer 2H-SnS2. *Sci. Rep.* **2018**, *8*, 10194.

(16) Puretzky, A. A.; Liang, L.; Li, X.; Xiao, K.; Wang, K.; Mahjouri-Samani, M.; Basile, L.; Idrobo, J. C.; Sumpter, B. G.; Meunier, V.; Geohegan, D. B. Low-Frequency Raman Fingerprints of Two-Dimensional Metal Dichalcogenide Layer Stacking Configurations. *ACS Nano* **2015**, *9*, 6333−6342.

(17) Dhar, L.; Rogers, J. A.; Nelson, K. A. Time-resolved vibrational spectroscopy in the impulsive limit. *Chem. Rev.* **1994**, *94*, 157−193.

(18) Merlin, R. Generating coherent THz phonons with light pulses. *Solid State Commun.* **1997**, *102*, 207−220.

(19) Domingue, S. R.; Winters, D. G.; Bartels, R. A. Time-resolved coherent Raman spectroscopy by high-speed pump-probe delay scanning. *Opt. Lett.* **2014**, *39*, 4124−4127.

(20) Raanan, D.; Audier, X.; Shivkumar, S.; Asher, M.; Menahem, M.; Yaffe, O.; Forget, N.; Rigneault, H.; Oron, D. Sub-second hyper-spectral low-frequency vibrational imaging via impulsive Raman excitation. *Optics letters* **2019**, *44*, 5153−5156.

(21) Smith, D. R.; Shivkumar, S.; Field, J.; Wilson, J. W.; Rigneault, H.; Bartels, R. A. Nearly degenerate two-color impulsive coherent Raman hyperspectral imaging. *Opt. Lett.* **2022**, *47*, 5841−5844.
(22) Smith, D. R.; Field, J. J.; Winters, D. G.; Domingue, S. R.; Rininsland, F.; Kane, D. J.; Wilson, J. W.; Bartels, R. A. Phase noise limited frequency shift impulsive Raman spectroscopy. *APL Photonics* **2021**, *6*, 026107.
(23) Raanan, D.; Lüttig, J.; Silberberg, Y.; Oron, D. Vibrational spectroscopy via stimulated Raman induced Kerr lensing. *APL Photonics* **2018**, *3*, 092501.
(24) Wahlstrand, J. K.; Merlin, R.; Li, X.; Cundiff, S. T.; Martinez, O. E. Impulsive stimulated Raman scattering: comparison between phase-sensitive and spectrally filtered techniques. *Opt. Lett.* **2005**, *30*, 926−928.
(25) Wilson, J. W.; Schlup, P.; Bartels, R. A. Synthetic temporal aperture coherent molecular phase spectroscopy. *Chem. Phys. Lett.* **2008**, *463*, 300−304.
(26) Schlup, P.; Wilson, J. W.; Bartels, R. A. Sensitive and Selective Detection of Low-Frequency Vibrational Modes Through a Phase-Shifting Fourier Transform Spectroscopy. *IEEE J. Quantum Electron.* **2009**, *45*, 777−782.
(27) Wilson, J. W.; Schlup, P.; Bartels, R. Phase measurement of coherent Raman vibrational spectroscopy with chirped spectral holography. *Opt. Lett.* **2008**, *33*, 2116−2118.
(28) Peterson, W.; De Pablo, J. G.; Lindley, M.; Hiramatsu, K.; Goda, K. Ultrafast impulsive Raman spectroscopy across the terahertz−fingerprint region. *Adv. Photonics* **2022**, *4*, 016003.
(29) van Dijk, M. A.; Lippitz, M.; Orrit, M. Detection of acoustic oscillations of single gold nanospheres by time-resolved interferometry. *Physical review letters* **2005**, *95*, 267406.
(30) Schlup, P.; Wilson, J.; Hartinger, K.; Bartels, R. A. Dispersion balancing of variable-delay monolithic pulse splitters. *Applied optics* **2007**, *46*, 5967−5973.
(31) Ghosh, S.; Herink, G.; Perri, A.; Preda, F.; Manzoni, C.; Polli, D.; Cerullo, G. Broadband optical activity spectroscopy with interferometric Fourier-transform balanced detection. *ACS photonics* **2021**, *8*, 2234−2242.
(32) Bartels, R. A.; Weinacht, T. C.; Wagner, N.; Baertschy, M.; Greene, C. H.; Murnane, M. M.; Kapteyn, H. C. Phase Modulation of Ultrashort Light Pulses using Molecular Rotational Wave Packets. *Phys. Rev. Lett.* **2001**, *88*, 013903.
(33) Gershgoren, E.; Bartels, R. A.; Fourkas, J. T.; Tobey, R.; Murnane, M. M.; Kapteyn, H. C. Simplified setup for high-resolution spectroscopy that uses ultrashort pulses. *Opt. Lett.* **2003**, *28*, 361−363.
(34) Wilson, J. W.; Bartels, R. A. Rapid birefringent delay scanning for coherent multiphoton impulsive Raman pump−probe spectroscopy. *IEEE J. Sel. Top. Quantum Electron.* **2012**, *18*, 130−139.
(35) Bartels, R. A.; Weinacht, T. C.; Leone, S. R.; Kapteyn, H. C.; Murnane, M. M. Nonresonant Control of Multimode Molecular Wave Packets at Room Temperature. *Phys. Rev. Lett.* **2002**, *88*, 033001.
(36) Ren, L.; Hurwitz, I.; Raanan, D.; Oulevey, P.; Oron, D.; Silberberg, Y. Terahertz coherent anti-Stokes Raman scattering microscopy. *Optica* **2019**, *6*, 52−55.


https://doi.org/10.1021/cbmi.4c00020
*Chem. Biomed. Imaging* 2024, 2, 584−591